



Experimental and scale-span numerical investigations in conventional and longitudinal torsional coupled rotary ultrasonic–assisted drilling of CFRPs

Yong Liu^{1,2} · Zitao Pan¹ · Qiannan Li¹ · Zhenchao Qi² · Wenliang Chen²

Received: 17 May 2021 / Accepted: 24 October 2021 / Published online: 29 November 2021
© The Author(s), under exclusive licence to Springer-Verlag London Ltd., part of Springer Nature 2021

Abstract

Longitudinal torsional coupled rotary ultrasonic–assisted drilling (LTC-RUAD) technology is introduced to improve the surface roughness of the hole-wall and solve the tear, burr, and delamination of carbon fiber–reinforced polymers (CFRPs) induced by large thrust force and torque during conventional drilling (CD). An experiment and scale-span numerical investigation of drilling CFRPs were presented for both the CD and LTC-RUAD processes in this study. A drilling experimental platform using the LTC-RUAD was built via a novel independently designed and manufactured LTC-RUAD vibration actuator, while the drilling experiments involving T700S-12 K/YP-H26 CFRP specimens with different process parameters were carried out by adopting the different ultrasonic vibration amplitude (UVA) in the longitudinal and torsional directions. Then, a three-dimensional (3D) scale-span FE simulation model of the CD and LTC-RUAD which applied the different UVA using tapered drill-reamer (TDR) is developed to find more details about the effects of machining quality of the holes. Experimental and simulation results revealed that the maximum average thrust force reduction is observed to be as high as 30% under certain drilling conditions, and the maximum average thrust force and the delamination factor of the drilled hole shows a “concave” trend with the increase of the UVA. The quality at the exit of the drilled hole is best when adopting $S_r = 2000$ rpm, $S_f = 0.01$ mm/rev, $A_{\text{lon}} = 7.02$ μm , and $A_{\text{tor}} = 9.29$ μm in the LTC-RUAD. The delamination factor is only 0.054, and the damage factors are reduced by 69.67% compared with CD.

Keywords CFRPs · Drilling · Scale-span · LTC-RUAD · Ultrasonic vibration amplitude

1 Introduction

Carbon fiber–reinforced polymers (CFRPs) are being widely used in aerospace industry, automobile industries, and several other structural applications owing to their superior mechanical and physical properties [1, 2]. Although a near-net shape process is usually for CFRP components, additional machining operations are often required to facilitate

furtherly the installation of rivets or bolted joints. For any mechanical fastening, conventional drilling (CD) process is extensively used for producing CFRP holes. However, different to drill metal materials, various mechanical damages in terms of delamination, poor surface integrity, fiber pullout, fiber breakage, and burr usually occur due to heterogeneous and anisotropic nature of CFRP laminates during drilling [3, 4]. These undesirable drilling-induced damages not only directly deteriorate the surface finish and assembly tolerance, but also reduce the hole strength against fatigue, leading to reducing the load-carrying capacity of CFRP structure [5]. To overcome the aforementioned problems, a need for a less invasive drilling technique capable to mitigate damage in drilling CFRP structural components is recognized.

A hybrid non-traditional process, known as “rotary ultrasonic–assisted drilling (RUAD),” has been successfully extended to the area of CFRP drilling owing to its remarkable improvement in machinability for machining difficult-to-machine metal material in the last few years [6,

✉ Yong Liu
liuyong.1991.happy@just.edu.cn

✉ Zhenchao Qi
qizhenchao2007@foxmail.com

¹ College of Mechanical Engineering, Jiangsu University of Science and Technology, Zhenjiang 212003, People’s Republic of China

² College of Mechanical and Electrical Engineering, Nanjing University of Aeronautics and Astronautics, Nanjing 210016, People’s Republic of China

7]. In the RUAD, high-frequency vibrations, typically in the range of 20 kHz, generated by a piezoelectric transducer are superimposed on a rotating standard tool in the axial direction or rotational direction to improve the machining process [8]. Fundamentally, the RUAD is a completely different process from CD, and the tool-workpiece interaction is intermittent with significantly higher deformation rates. Nonetheless, the cutting process is continuous in CD. Compared with CD, the RUAD is shown to be beneficial for drilling holes in brittle materials [9] and has many documented advantages, for instance, reduction in thrust force, improved surface finish, better hole quality, burr elimination, and lower tool wear [10].

In the literature, some researchers have conducted the RUAD experiments to investigate the effects of different drill bit geometries and process parameters on damage defects of drilled holes. Sadek et al. [11] investigated the RUAD process to reduce thermal and mechanical defects associated with drilling of CFRPs; the results revealed that the optimized RUAD condition can reduce the machining temperature by 50% and the thrust force by 40% and produce delamination-free holes, without affecting productivity. Cong et al. [12] employed the similar RUAD method to drill CFRP laminate to prevent clog and improve the quality of hole. Wang et al. [13, 14] also successfully extended the RUAD method in which vibration is applied along the tool axis to improve the machining of CFRP surfaces, whereas the risk of delamination damage increases since the cooling fluid with a certain pressure is pumped through a core drill. Thomas et al. [15] investigated the vibrational characteristic of twist bit; the experimental and simulation results showed that there are several well-documented advantages of the RUAD over CD techniques such as reduction in thrust forces and torque, better surface finish, low tool wear, and elimination/reduction in burr formation. Makhadmeh et al. [16] conducted an extensive experiment by using high-frequency vibration to excite a drill bit during its standard operation to study the effect of the RUAD on CFRPs; the research results showed that adopting the RUAD technique had a more significant effect on improving the drilling quality compared with CD. Asami et al. [17] developed a LTC vibration device for ultrasonic machining of brittle materials with an abrasive slurry. Compared with the one-dimensional longitudinal vibration drilling, the LTC vibration was discovered to improve the machining efficiency. These above studies showed that several advantages of the RUAD such as reduction in drilling forces and torque, better surface finish, low tool wear, and elimination in burr formation were existed when compared CD.

Although experimental efforts have been done about the use of the RUAD in the drilling of CFRPs, still some considerable works remain so that this strategy can be industrialized efficiently. Accordingly, finite element (FE) simulation is a helpful approach to evaluate this machining process in detail [18]. Except for few literatures reported by Phadnis et al. [19, 20] in simulation of cutting forces in the RUAD; there are not any

corresponding research representing burr formation, delamination generation, and tool movement in the simulation of vibration drilling owing to the complexity involved in modeling of such processes and the extent of computational resources required. In aforementioned studies, they indicated that the average thrust force in the RUAD reduced as high as 30% compared to CD of CFRPs. Furthermore, it was noted that the predicted results were in good agreement with experimental results.

However, in the numerical analysis for CFRPs drilling using the RUAD, almost all of them used macro-mechanics theories (Tsai-Wu [21], Hashin [22, 23], Puck [24] and Chang-Chang [25], etc.) though they were capable to determine the damage modes by regarding composite as homogeneous material, where some real damage defects are impossible to be simulated, such as burr. In addition, CFRPs is a kind of multiphase material with macro–micro characteristic, whereas these theories did not consider the influence of local stress difference caused by different mechanical performances of constituent fiber and matrix, which are related to the behaviors of CFRPs at macroscale. For the drilling FE model, the stress and strain of CFRP laminate in the direction of thickness, which is lack of consideration in these macro-mechanics theories, should be considered in particular. If the microscale modeling method of the CFRP FE model is adopted, the computing power and efficiency in a high-performance workstation will be two important factors that limit its development.

Meanwhile, as one of two major variables of the RUAD, the ultrasonic vibration amplitude (UVA) in longitudinal and torsional directions plays a dominant role in longitudinal torsional coupled rotary ultrasonic-assisted drilling (LTC-RUAD) process. The influence of machining quality on drilled holes is not researched furtherly as the change of the UVA. Plentiful of studies are majorly focused on the “abrasive drilling” in terms of optimizing the process parameters, whereas the drilling and grinding-coupled process is not researched further in the drilling of CFRPs. For instance, tapered drill-reamer (TDR) or step drill bit is adopted in the LTC-RUAD process for CFRP drilling.

Thus, this study presents an experiment and scale-span numerical investigation of drilling in a CFRPs for both CD and LTC-RUAD processes by modifying different UVA in the longitudinal and torsional directions. First, a drilling experimental platform is built based on the novel independently designed and manufactured LTC-RUAD vibration actuator, while drilling experiments involving T700S-12 K/YP-H26 CFRPs specimens with different process parameters are carried out by modifying the UVA in the longitudinal and torsional directions. Meanwhile, a three-dimensional (3D) scale-span FE simulation model of CD and LTC-RUAD, which applied different UVA using TDR, is developed to find more details about the effects of machining quality of the holes. Finally, the defect suppression mechanism of CFRP hole in LTC-RUAD is revealed via FE simulation results from the perspectives of thrust force and torque, burr, and delamination at the hole exit. In addition, the correlative factors affecting

the hole-making quality, hole-making defects, and cutting force of CFRPs to optimize process parameters and LTC parameters, which is conducive to achieve high-precision drilling.

2 Experimental setup and conditions

2.1 LTC-RUAD test system and calibration

LTC-RUAD experimental instruments used in this paper are attributed to be designed and manufactured by Nanjing University of Aeronautics and Astronautics independently. The whole LTC-RUAD test system consists of BT40 LTC ultrasonic vibration holder, labview controller, power supply, and the corresponding voltage amplifier. LTC ultrasonic vibration holder is majorly comprised of longitudinal torsional coupler, electrode slice, piezoelectric ceramic piece, and amplitude amplifier pole, etc. Actual parts and connection relationship of each parts are shown in Fig. 1.

Before the experiment, it is necessary to calibrate the amplitude and resonant frequency of longitudinal and torsional vibration of the cutter according to the extended length of TDR bit. Resonance frequency of the LTC experimental system is calibrated at the initial voltage, and different

voltages are applied to the tool handle to control different UVAs. As shown in Fig. 1, the calibration process of longitudinal and torsional amplitudes is completed by real-time monitoring of micro-displacement sensor that is produced by HangZhou Oriental Gauge Technology Co., Ltd.

Figure 2 presents the amplitude change curves of TDR bit in the longitudinal and torsional directions at different frequencies and voltages when the length of the transverse blade from the ER nut is approximately 40 mm. The resonant frequencies of longitudinal and torsional amplitudes are not consistent under different voltages, and the resonance amplitudes are larger in longitudinal and torsional directions when the frequency is about 19.6 kHz, as shown in Fig. 2(a). Simultaneously, the amplitude of longitudinal vibration and torsional vibration shows a semi-linear relationship at the resonant frequency, and it is different from the original design which is supposed to be linear, as shown in Fig. 2(b). The primary reason for such errors is that the piezoelectric ceramic piece has hysteresis and creep properties, etc.

2.2 LTC-RUAD experimental procedure of drilling CFRP laminate

A corresponding CFRP with a thickness of 5.76 mm (32 layers) was used for conducting the drilling experiments in this

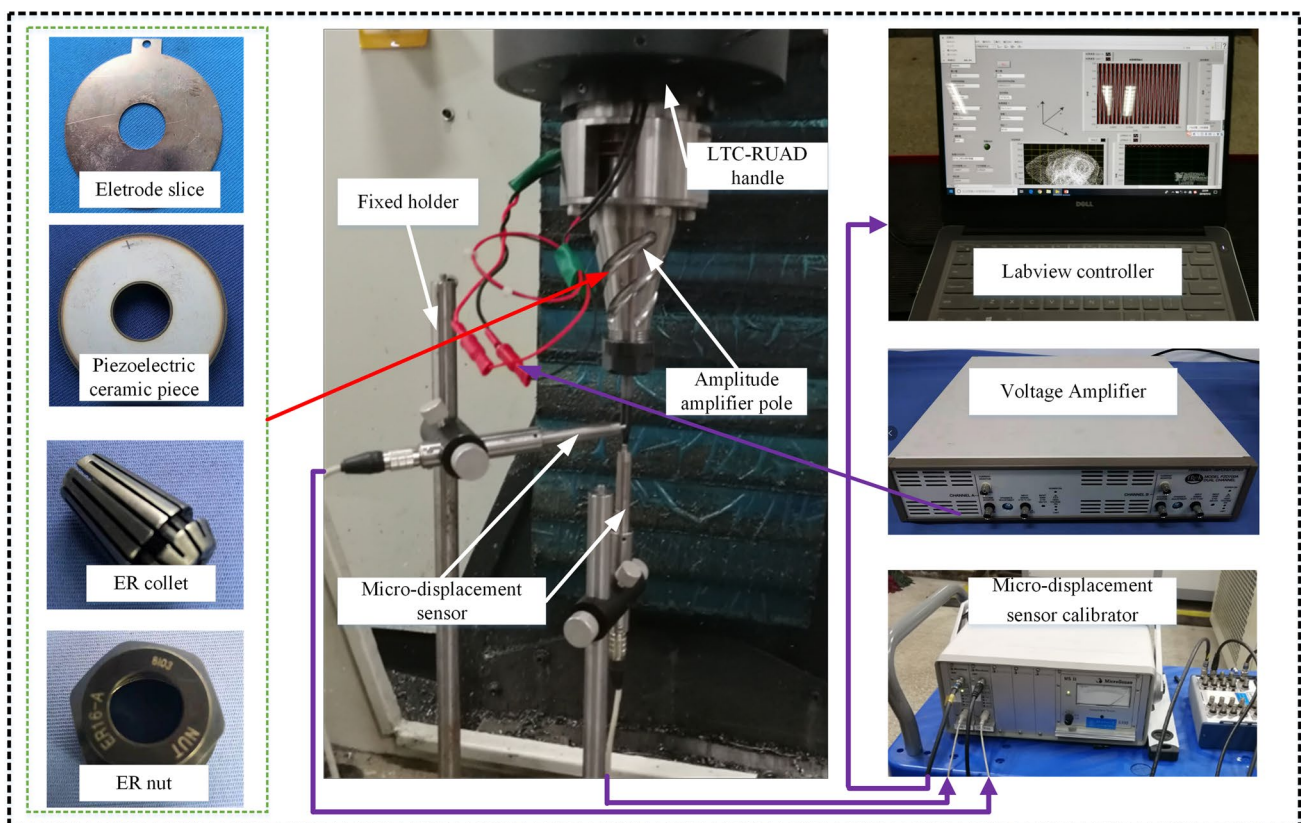


Fig. 1 LTC-RUAD handle and ultrasonic amplitude calibration

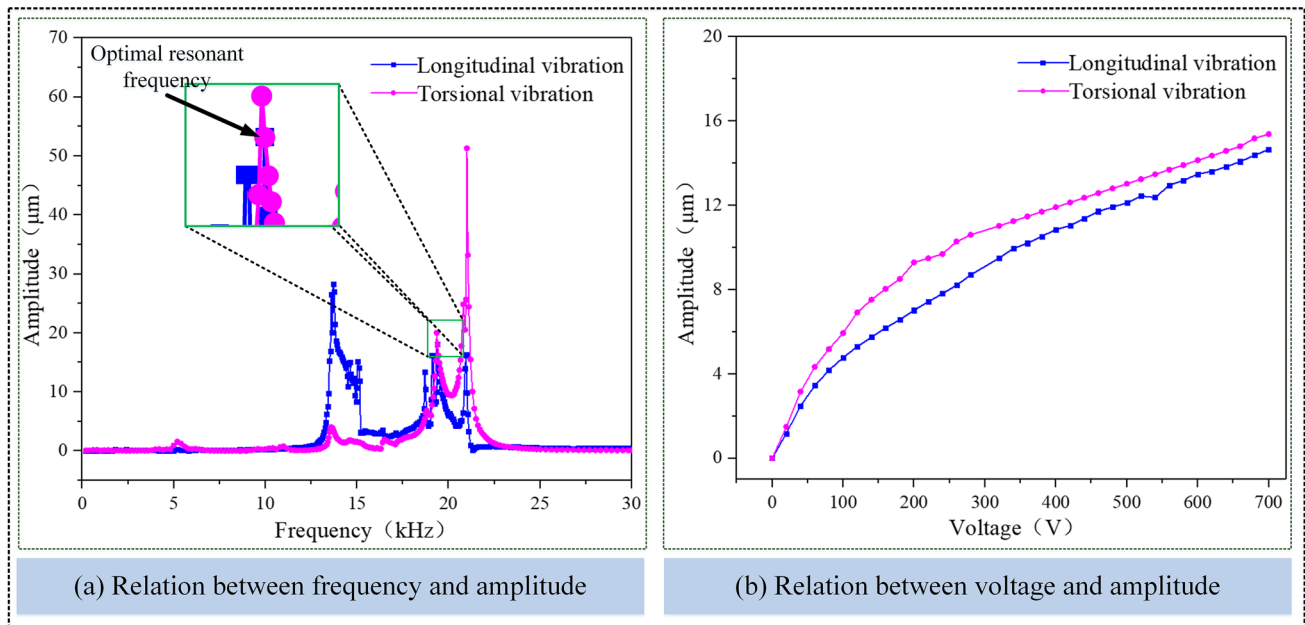


Fig. 2 Frequency-amplitude and voltage-amplitude diagrams. **(a)** Relation between frequency and amplitude. **(b)** Relation between voltage and amplitude

study. The CFRPs were made using unidirectional prepreps supplied by GW Composite Co., Ltd., and the model of prepreps was T700S-12 K/YP-H26. The curing process mainly followed the literature [26] (Fig. 3). The fiber volume fraction after curing was approximately 59%. The entire curing process was performed in the composite material forming laboratory of Nanjing University of Aeronautics and Astronautics. After curing, CFRPs were made into the dimension of the drilling specimen via waterjet cutting, for which the length and width of specimens were 180 mm and 120 mm, respectively.

The entire schematic diagram of the experimental setup and the specific experimental setup are illustrated in Figs. 4 and 5. It mainly consists of an LTC-RUAD system and a data acquisition system. CFRPs were mounted on a dynamometer using a special fixture on the table of a XK7124 CNC machining center, and the TDR bit, which is installed on the LTC-RUAD handle, was fed into the CFRPs. Drilling experiments were carried out on CFRPs using a diameter of Φ 6-mm cemented carbide TDR bit,

and the corresponding structural parameters are shown in Fig. 3 and Table 1. Experiments were conducted without coolant. The thrust force was measured by using a piezoelectric dynamometer (type Kistler 9257B) during drilling. The charge amplifier (type Kistler 5407A) converted the resulting charge signals, which were proportional to the force, to voltage and managed the experiment through the data acquisition system (type NI DAQ).

A full factorial design of experiments with two factors based on the initial process parameters was adopted in this study [27]. Three levels of spindle feed rate and their corresponding spindle rotation speed were employed. According to the amplitude of the calibration curve shown in Fig. 2, the torsional UVA and longitudinal UVA were corresponding to each other under the same voltage owing to the resonance amplitude which was inspired by the same piezoelectric ceramic piece. Therefore, different UVAs generated under different voltages were adopted according to the optimal resonant frequency of LTC-RUAD handle. The integrated machining scheme is shown in Table 2.

Fig. 3 Geometrical structure of TDR. **(a)** Basic structure. **(b)** Geometrical parameters

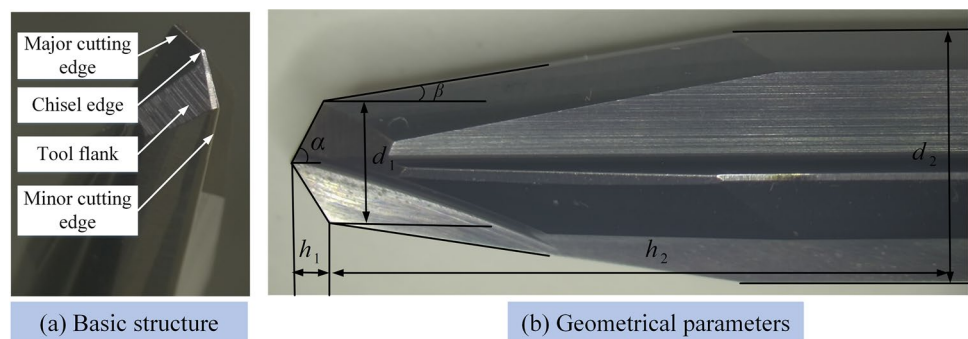
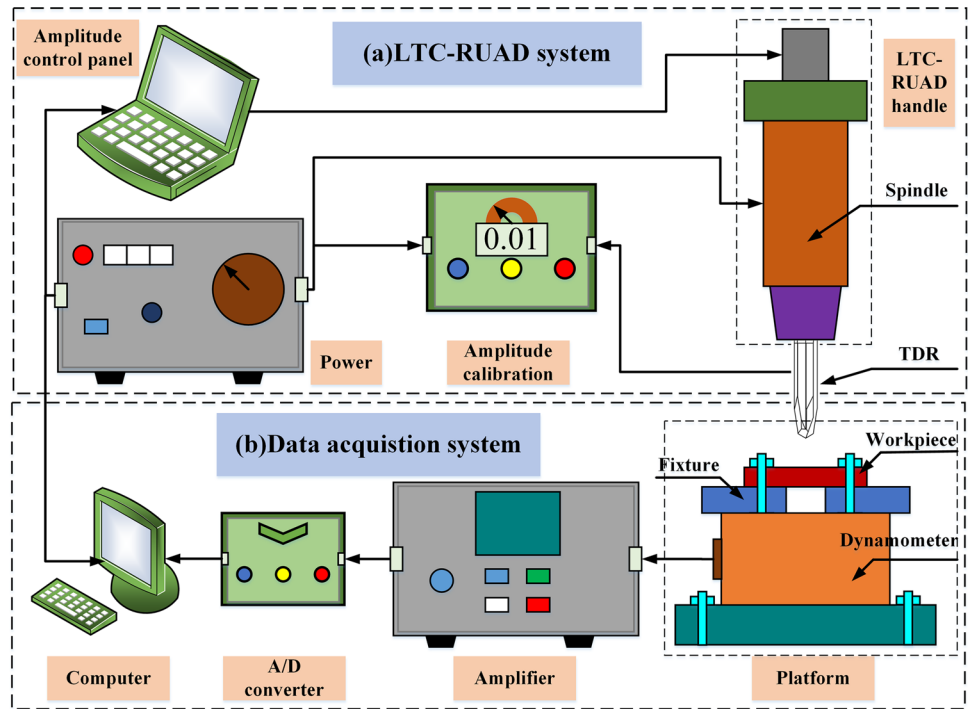


Fig. 4 Schematic diagram of LTC-RUAD experimental setup. (a) LTC-RUAD system. (b) Data acquisition system



Experiments of each machining parameter were repeated 3 times to obtain a satisfactory measured dataset. All the experiments were carried out on the LTC-RUAD handle. For instance, the voltage was 0 V in CD. In addition, a new TDR bit was employed for the sake of removing the influence of tool wear during drilling. All process experiments were performed using three laminates. Finally, as shown in Fig. 13, the hole’s damage of CFRP specimens was observed through a scanning electron microscope (SEM) produced by HiROX Co., Ltd., after waterjet cutting, such as delamination and burr.

3 Scale-span finite element analysis of drilling in CFRPs using LTC-RUAD

3.1 Principle of the LTC-RUAD process of CFRPs using TDR

The structure of TDR mainly contains three parts: chisel edge, major cutting edge, and leading edge of a land (minor cutting edge) [28]. The cutting process of the bit is rotary and the feed

Fig. 5 LTC-RUAD experimental setup for drilling T700S-12 K/Y-PH26

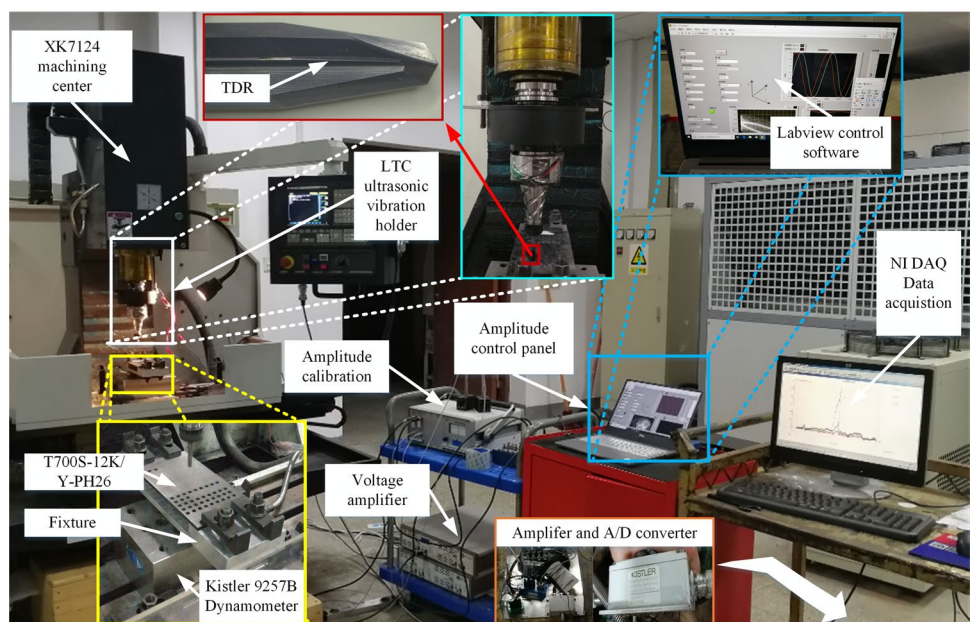


Table 1 Parameters of TDR bit

Basic parameters		Geometrical parameters	
Model	K40	α	118°
Materials	Cemented carbide	β	8.5°
Coating	AlTiN	d_1	4 mm
Coating thickness	2 μm	d_2	6 mm
Work length	25 mm	h_1	1.2 mm
Total length	32.5	h_2	18.5 mm

motion is located at the axial direction in the CD of CFRPs, respectively. The major cutting edge is the drilling process that is mainly to achieve material removal, while the minor cutting edge is the process of cutting residual material which would achieve the role of reaming. Adopting this structural design is helpful to improve the machining efficiency. The thrust force is mainly determined by chisel edge owing to the chisel edge squeezing the workpieces during drilling, and the torque is generated by the major cutting edge and minor cutting edge according to the cutting thickness of the single rotary.

In LTC-RUAD, the LTC vibration of the TDR bit for hole drilling of CFRPs is applied. Figure 6(a) shows the kinematic view of LTC-RUAD. Clearly, a polar coordinate is defined on the TDR bit end face. The moving trajectory of position r from the center of TDR bit can be written as follows.

$$\begin{cases} L = -A_{tor}\sin(2\pi ft) - 2\pi r S_r t \\ R = r \\ Z = -A_{lon}\sin(2\pi ft) - S_f [2\pi f A_{tor} \cos(2\pi ft) + S_r] t \end{cases} \quad (1)$$

where L , R , and Z denote the kinematic position of the drilling. A_{tor} and A_{lon} denote the UVA of torsional vibration and longitudinal vibration, respectively. The parameter f denotes the ultrasonic frequency, t denotes the time, r denotes the displacement from the center of TDR bit, S_r denotes rotational speed due to the TDR rotation, and S_f denotes the feed rate of TDR bit.

Simultaneously, as shown in Fig. 6(b), the circumferential angular displacement β of the TDR can be written as:

$$\beta = L/r \quad (2)$$

The displacements at each point in TDR can be expressed as:

$$\begin{cases} x = r^* \cos[(-A_{tor}\sin(2\pi ft) - 2\pi S_r t)/r] \\ y = r^* \sin[(-A_{tor}\sin(2\pi ft) - 2\pi S_r t)/r] \\ z = -A_{lon}\sin(2\pi ft) - S_f [(2\pi f A_{tor} \cos(2\pi ft) + S_r)] t \end{cases} \quad (3)$$

where x , y , and z denote the displacement in rectangle coordinate, respectively.

Figure 7(a) presents the calculated moving trajectory of the position r from the center of the TDR when $r = 3$ mm, $S_r = 2000$ rpm, $S_f = 0.01$ mm/rev, $A_{tor} = 10$ μm, $A_{lon} = 10$ μm, and $f = 19.6$ kHz. Figure 7(b) demonstrates the moving trajectory of TDR bit in LTC-RUAD (purple line) is rather different from the moving trajectory in the CD (blue line), longitudinal RUAD (orange line), and torsional RUAD (saffron yellow line) owing to the torsional vibration and longitudinal vibration of TDR bit. There are reciprocating effects in the axial and rotational directions when adopting the LTC-RUAD process, which means that the tool will lift and does not contact the material within a rotation period. The cure also indicates that the chip thickness of the cutting edge is not uniform, while the fibers can be cut off more quickly in the cutting direction. Besides, the softening of resin is promoted due to the reciprocating microscopic cutting, so that the surface topography of the hole may appear the obvious ironing phenomenon. Thus, the moving trajectory difference of the TDR in CD and LTC-RUAD would highly affect the corresponding machining performances.

3.2 Progressive failure theories of the scale-span model of CFRPs

The adopted modeling method in this paper is based on the implementation of dynamic micromechanics of failure (MMF) criterion of CFRPs. The kernel of this method consists of establishing the damage-failure constitutions of fiber and matrix under dynamic loading conditions and realizing damage-failure information interaction between the representative volume element (RVE) model which includes fiber and matrix and the macroscopic drilling FE model of CFRPs [29]. According to the scale-span FE drilling schematic

Table 2 Machining scheme

Parameters	CD	LTC-RUAD
Drilling depth (mm)	20	20
Spindle rotation speed (rpm)	2000, 3000, 4000	2000, 3000, 4000
Spindle feed rate (mm/rev)	0.01, 0.02, 0.03	0.01, 0.02, 0.03
Resonance frequency (kHz)	0	19.6
The UVA of longitudinal vibration A_{lon} (μm)	0	4.77, 6.14, 7.02, 7.81, 9.63, 10.14
The UVA of torsional vibration A_{tor} (μm)	0	5.94, 7.88, 9.29, 9.62, 10.73, 11.21

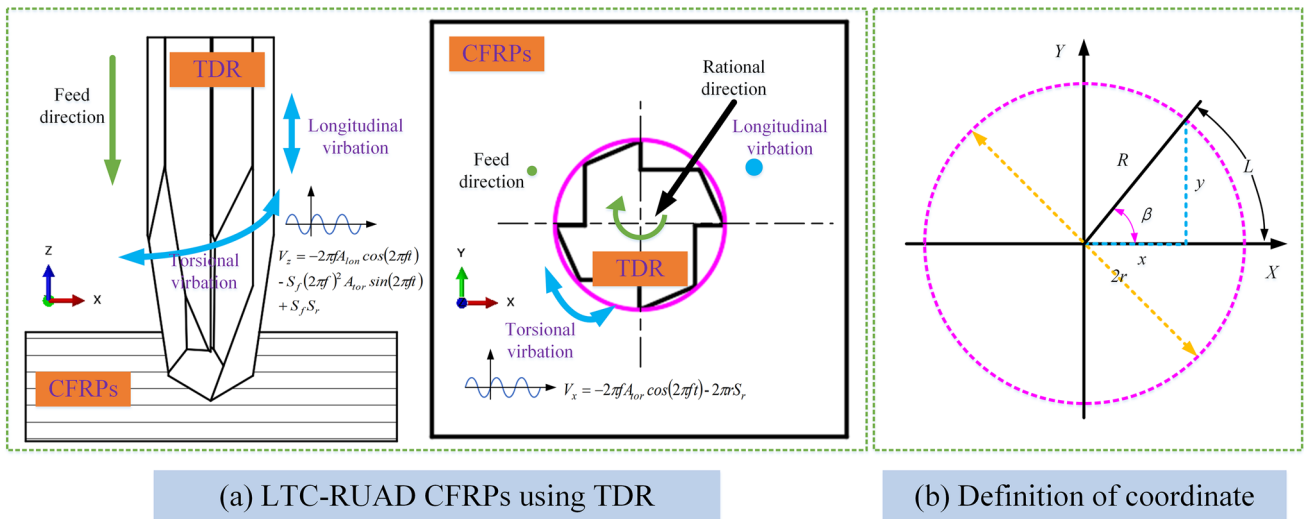


Fig. 6 Illustration of LTC-RUAD using TDR. (a) LTC-RUAD CFRPs using TDR. (b) Definition of coordinate

diagram shown in Fig. 8, the whole simulation process is mainly divided into three steps:

Step (1): Components of CFRPs are simplified as idealized multidirectional preset layup sequence structure which includes multilayer UD-CFRPs. It is assumed that the structure of multidirectional CFRPs (MD-CFRPs) is flawless and that the fibers and matrix are tightly bonded during curing. Some minor defects in the material are overlooked, such as voids and microcrack, which is shown in Fig. 8(c). Meanwhile, the drilling bit FE model is also required to be established according to the actual drilling conditions, which is shown in Fig. 8(a).

Step (2): The corresponding RVE model is also established via the basic parameter of CFRPs, such as the diameter of the filament fiber and the fiber volume fraction of CFRPs, as shown in Fig. 8(b). The stress–strain relationship of the damage element of the macroscopic FE model of CFRPs will be transferred to the RVE model via SAFs when the bit is in contact with CFRPs. These elements of fiber and matrix in the RVE model will be secondarily analyzed through the MMF criterion of CFRPs, including element failure judgement, stiffness degradation, and deletion. In addition, if the elements are not deleted in the current increment, the element with reduced stiffness will be

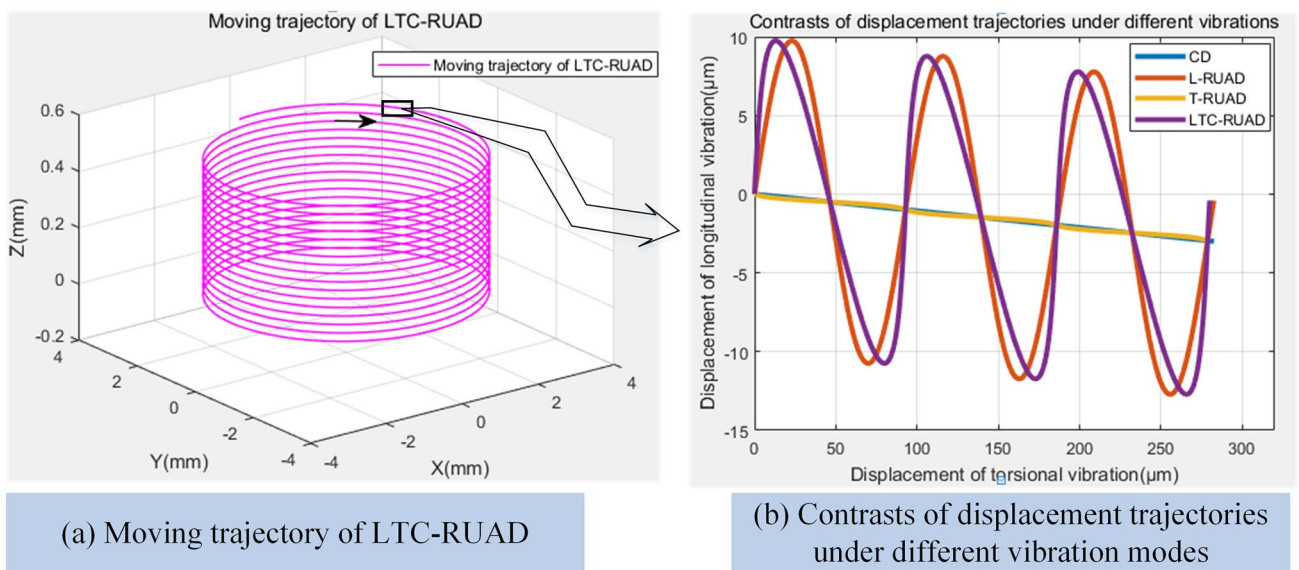


Fig. 7 Moving trajectory of TDR. (a) Moving trajectory of LTC-RUAD. (b) Contrasts of displacement trajectories under different vibration modes

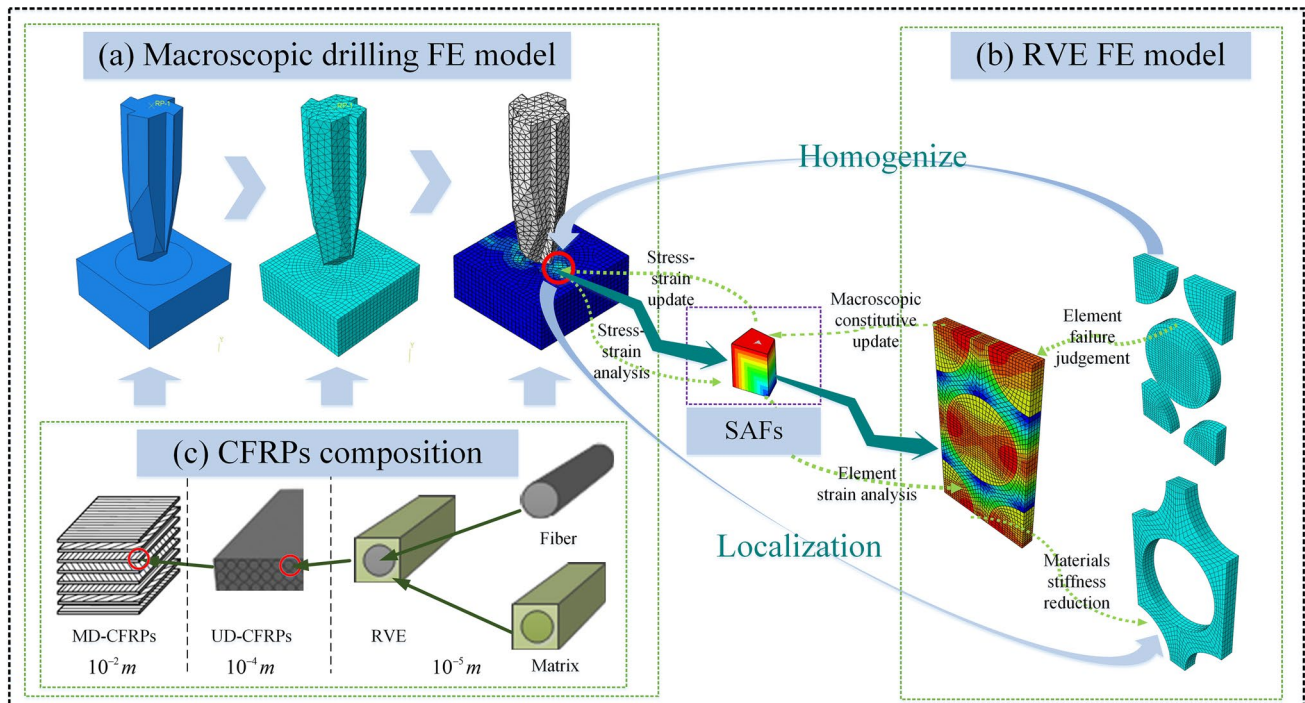


Fig. 8 Scale-span FE drilling schematic diagram. (a) Macroscopic drilling FE model. (b) RVE FE model. (c) CFRP composition

homogenized in macroscopic drilling FE model, and the macroscopic elastic properties of elements are characterized by the scale-span prediction method [30], which is used for analysis in the next iteration step.

Step (3): The macroscopic elastic properties of elements with different degrees of damage will be assigned to the corresponding macroscopic elements with different layup sequence structure of CFRPs. Then, the next iteration analysis of the macroscopic drilling FE model will be carried out, and the scale-span simulation process of drilling CFRPs will end if preset increments are reached.

3.3 Drilling scale-span FE modeling of CFRPs using LTC-RUAD

A 3D drilling FE model of corresponding CFRPs was established with the help of ABAQUS/Explicit software. The dynamic characteristics of the entire drilling process, which is accounted for the complex contact interaction between the TDR and CFRPs' surface, were characterized in the FE model. The newly developed 3D progressive damage-failure model, which is based on the MMF criterion explained in the literature, was used as user-defined material model for CFRPs to facilitate element deletion of mesh elements and simulate inter-ply delamination which suffered severe deformations. The corresponding span-scale FE model of drilling CFRPs and the parameters of the TDR are shown in Fig. 9.

High temperature-resistant CFRP (type T700S-12 K/YP-H26) laminates, which is the same type of composites that were used in the experiment, are used as the research object in the FE modeling. The fiber volume fraction is approximately 59%, and the layup sequence of the CFRPs is $[(0^\circ/90^\circ/45^\circ/-45^\circ)_4]$. Orthotropic material property was assigned to each UD-CFRP laminate according to the fiber orientation by using a predefined local coordinate system. The cohesive elements (CEs), which are modeled as having a thickness 0 mm, were used for simulating the delamination phenomenon. The material parameters of UD-CFRP laminate elements and cohesive-zone elements are reported in Tables 3 and 4, respectively.

The overall dimensions ($15 \text{ mm} \times 15 \text{ mm} \times 5.76 \text{ mm}$) of the laminated plate were modeled as CFRPs with an individual ply thickness of 0.18 mm. A cemented carbide (K40) coated with TDR bit of a diameter of $\Phi 6 \text{ mm}$ was modeled as a discrete rigid body to improve the computational efficiency required to discretize the complex bit geometry. A lumped mass and rotary inertia were applied at a reference point located at the top of the TDR bit for the sake of accounting for the thrust force of the entire drilling process. The reference point of the TDR was also assigned with a single node mass and rotary inertia element, where the axial velocity and rotations were loaded. A refined mesh was used in the immediate vicinity of the model volume to be drilled and a coarse mesh was used to discretize the volume away from the drilling zone for the sake of ensuring that the prediction of thrust force was more accurate and maximized the utilization of the available

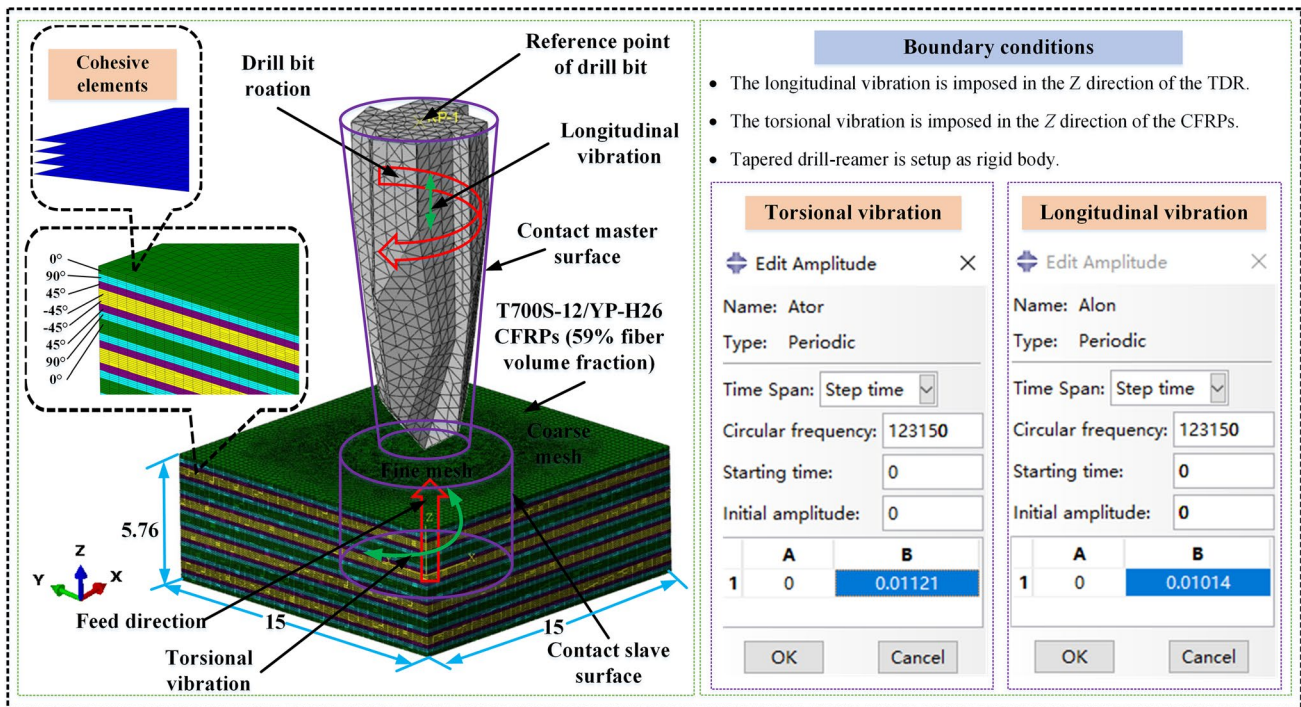


Fig. 9 Setup showing the FE model of drilling CFRPs using LTC-RUAD

computing resources during drilling. CFRPs were modeled using the C3D8R 8-node, 3D brick-reduced integration elements. The cohesive zone was modeled using the COH3D8 0-thickness CEs. Analogously, the TDR was modeled with the C3D10M 10-node, 3D discrete rigid elements. The whole FE model consisted of 3382122 elements, including 819108 CEs and 8208 tetrahedral elements in the model of the TDR, with the smallest element size of 40 μm.

As limited by the degree of freedom in the boundary condition set module of the ABAQUS software, the process parameters and LTC ultrasonic vibration parameters are required to setup separately, which is a little different from the actual working conditions. Velocity boundary conditions were used to account for dynamic characteristics of the entire drilling process. The spindle rotation was loaded at

the reference point located at the top of the TDR, namely the rotational motion is rotating around about the Z direction. Meanwhile, the reference point was constrained in X and Y directions, and the longitudinal vibration was imposed in the Z direction. Similarly, the feed rate was loaded at the CFRP workpiece, and the torsional vibration was imposed in the Z direction. The simulation machining scheme is consistent with the experimental machining scheme. For instance, the settings of the LTC parameters in the ABAQUS software are shown in Fig. 9; when the resonant frequency is 19.6 kHz, the torsional UVA is 11.21 μm and the longitudinal UVA is 10.14 μm.

A coulomb friction model was deemed appropriate, and the corresponding coefficient of friction of 0.3 was used in the FE model to analyze frictional effects during drilling simulation. A type of surface-to-surface kinematic contact algorithm in the ABAQUS/Explicit was employed to model penalty friction that based interaction between the TDR and CFRP models. The surfaces of TDR bit were set to the master surface, and elements that were located in a circular area with a diameter

Table 3 Material parameters used to model unidirectional CFRP laminate elements

Elastic parameters	Value (GPa)	Strength parameters	Value (MPa)
E_1	138.7	X^T/X^C	1870/1026
$E_2 = E_3$	7.04	Y^T/Y^C	45/156
$\nu_{12} = \nu_{13}$	0.25	Z^T/Z^C	40/145
ν_{23}	0.31	S_{XY}	87
$G_{12} = G_{13}$	2.959	S_{XZ}	87
G_{23}	2.505	S_{YZ}	58

Table 4 Material parameters used to model interface CEs

Stiffness	Value (N/mm ³)	Strength parameters	Value (MPa)	Fraction energy	Value (N/mm)
K_n	4×10^6	δ_n	60	G_n	0.2
$K_s = K_t$	1×10^6	$\delta_s = \delta_t$	90	$G_s = G_t$	1

of approximately 10 mm at the center of the CFRPs were assumed to be the slave surface to save computation time.

Based on the aforementioned settings, jobs were created and the corresponding calculation input file was output to check for errors. The mass scaling factor was set to 10^3 according to the reference [31] to improve computational efficiency on the premise of ensuring accuracy through many attempts. The complete computation of a job required approximately 192 h on a high-performance computer with two 48-core 8160 platinum processors and 128-GB RAM. All simulations were performed at the high-performance computing facility at Nanjing University of Aeronautics and Astronautics.

4 Results and discussion

For the sake of allowing a better comparison of the experimental and simulated thrust force, torque, and damages in entrance, hole-wall, and exit of the performed hole using CD and LTC-RUAD, a typical feed rate of $S_f=0.03$ mm/rev was chosen from the experimental feed data with a spindle speed $S_r=2000$ rpm. Meanwhile, LTC-RUAD experimental results

of other process parameters were also adopted to further evaluate the correctness of simulation results from the maximum average thrust force, torque, and delamination factor, etc.

4.1 Thrust force and torque

Figure 10 shows the experimental and simulated data for the thrust force in drilling of T700S-12 K/YP-H26 CFRP laminate using CD and LTC-RUAD in the entire drilling period. Apparently, the thrust force and torque prediction results of the drilling FE model are closely corresponding with experiments in eight stages according to the effects between TDR and CFRPs. The variation trend is almost consistent with the comparison of CD owing to the same initial process parameters which are adopted during drilling using the LTC-RUAD. Nonetheless, at the same period, there is a great difference in the transient amplitude of variation change ΔF though the maximum value which is greater than that of adopted CD according to the experimental results using the LTC-RUAD. The overriding reason is that the cutting process that exists

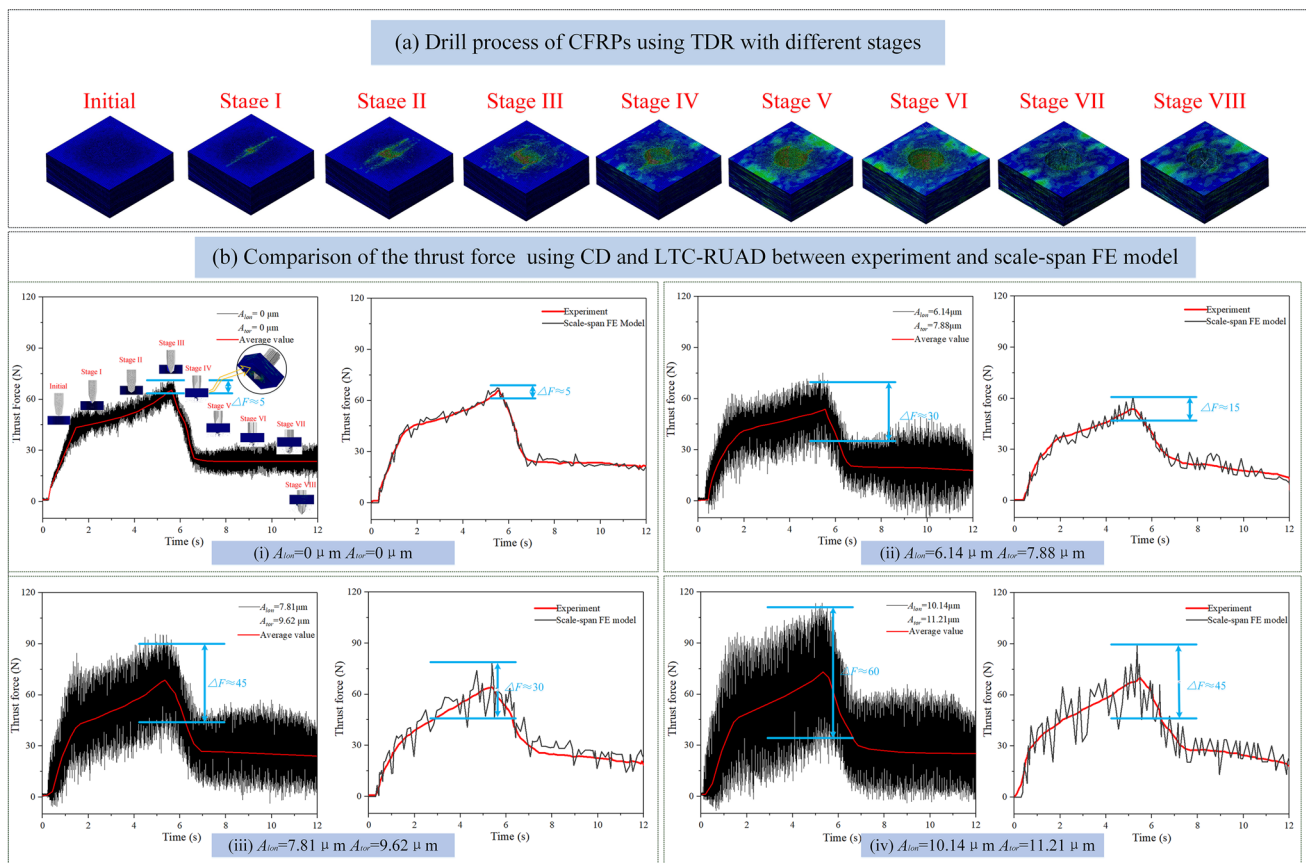


Fig. 10 Comparison of the thrust force using CD and LTC-RUAD. (a) Drill process of CFRPs using TDR with different stages. (b) Comparison of the thrust force using CD and LTC-RUAD between experiment and scale-span FE model

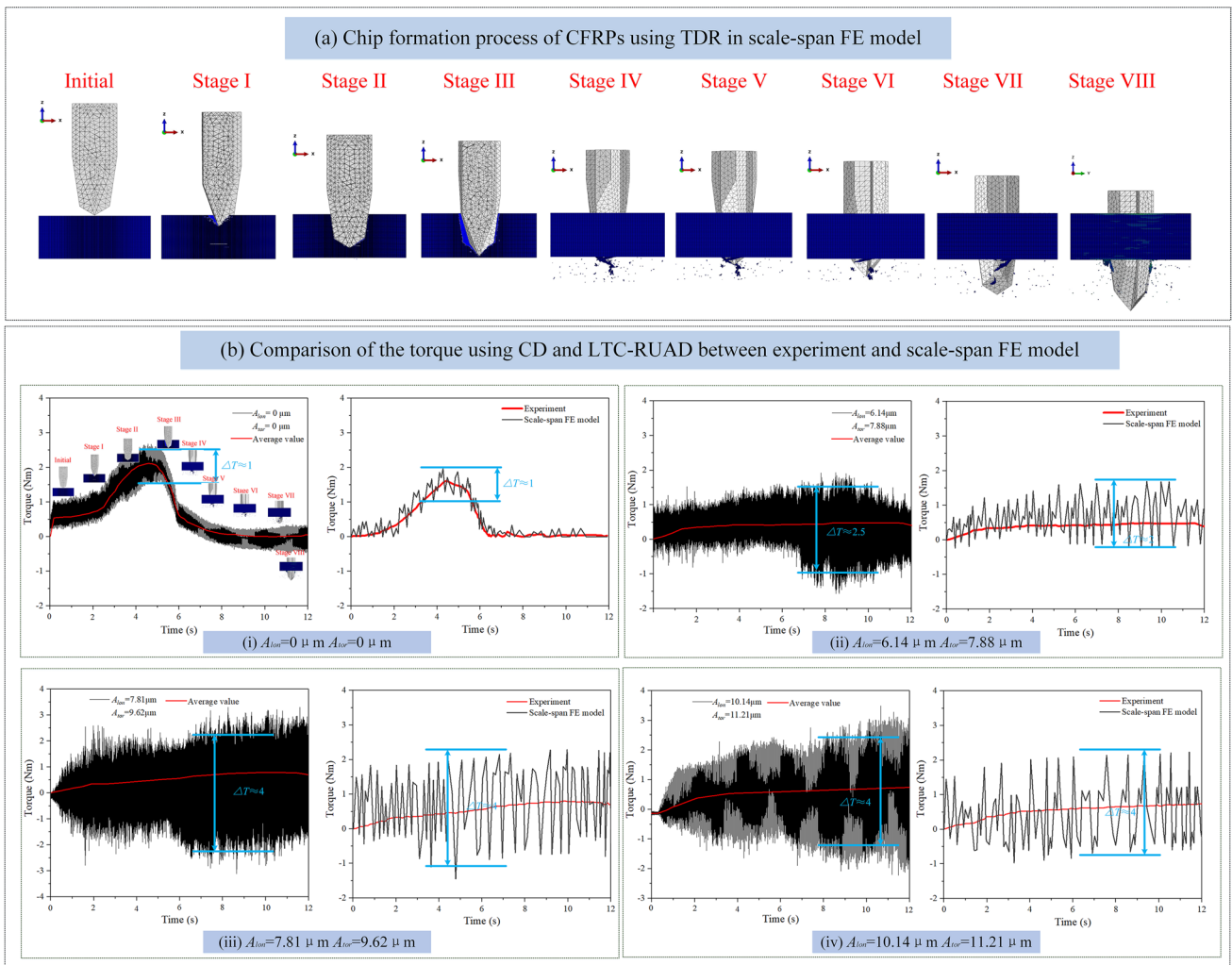


Fig. 11 Comparison of the torque using CD and LTC-RUAD. (a) Chip formation process of CFRPs using TDR in scale-span FE model. (b) Comparison of the torque using CD and LTC-RUAD between experiment and scale-span FE model

impacts characteristics at the microscale level according to the analysis of the principle of the LTC-RUAD process of CFRPs using TDR, which helps to reduce the

fracture toughness of fibers in the contact area, and then can cut them off quickly. Meanwhile, in the scale-span FE model, the elements located in contact area occurred

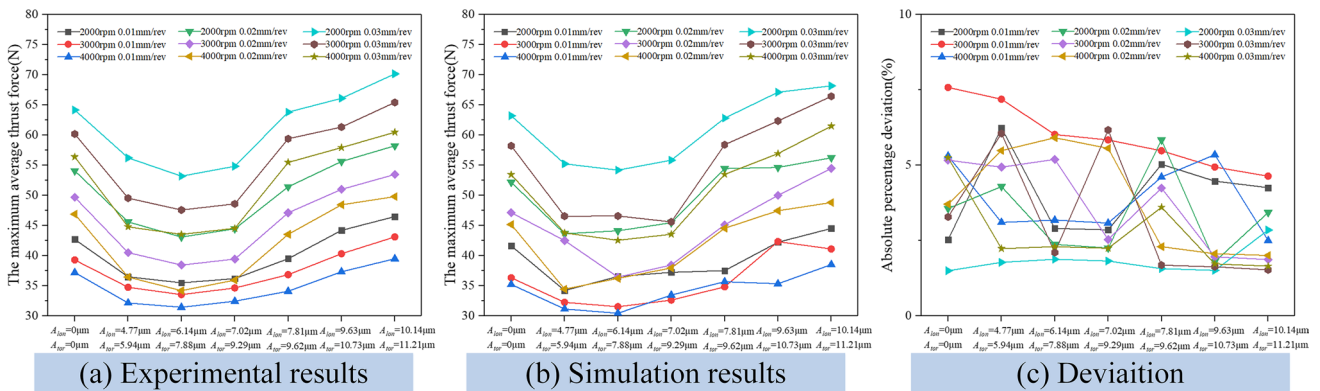


Fig. 12 Comparison of the maximum average thrust force and deviation. (a) Experimental results. (b) Simulation results. (c) Deviation

to fail rapidly and will be deleted, and the deleted elements are unrecoverable. Compared with the LTC-RUAD experimental results, the variation of instantaneous thrust force and its amplitude is smaller, whereas the maximum average thrust force is also smaller in the scale-span FE model. Nevertheless, the vibration amplitude of the scale-span model is smaller than that of the experimental results because of the differences between the scale-span FE model and the microscopic cutting model. For instance, the transient amplitude of variation changes $\Delta F \approx 60$ N in LTC-RUAD experiment, whereas the $\Delta F \approx 45$ N in the corresponding scale-span FE model when the $A_{tor} = 10.14 \mu\text{m}$, $A_{lon} = 11.21 \mu\text{m}$, as shown in Fig. 10(b).

Figure 11(a) presents the chip formation process of CFRPs using the TDR in scale-span FE model. The chip of CFRPs is generated primarily as the main cutting edge of the bit drills out of the bottom layer, and the value of the thrust force and torque decreased significantly. Similarly, Fig. 11(b) presents experimental and simulation results for the torque that adopts the LTC-RUAD with different UVA of the LTC vibration. Analogously, at the same period, there is also a great difference in the transient amplitude of variation change ΔT . However, the vibration change of the torque can be clearly distinguished at different stages because torsional vibration of the TDR bit is not existed in CD. According to the same reason as explained by the thrust force, the vibration

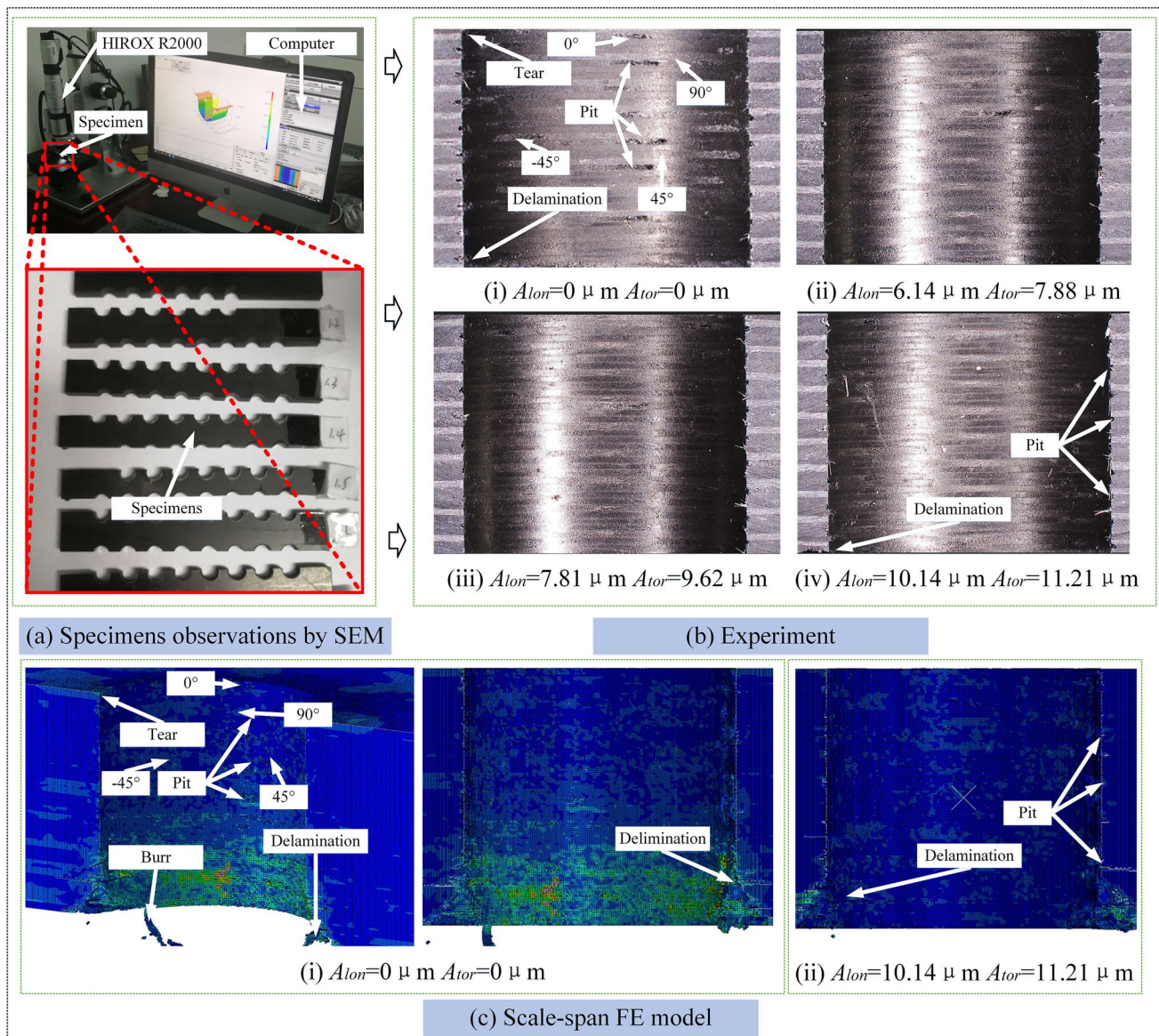


Fig. 13 Comparison of the visualized damage phenomenon with CD and LTC-RUAD. (a) Specimen observation by SEM. (b) Experiment. (c) Scale-span FE model

amplitude of scale-span model is slightly smaller than that of the experimental results owing to the differences between the scale-span FE model and the microscopic cutting FE model.

In order to evaluate the simulation results of the scale-span FE model accurately, the maximum average thrust force (obtained for the period of complete drill engagement) and the corresponding absolute percentage deviation are gathered among all the machining parameters, which is shown in Fig. 12. The maximum average thrust force could be realistically predicted via the established scale-span FE model in drilling of CFRPs using the LTC-RUAD, and the maximum deviation of the thrust force is only 7.58% among all process parameters compared with experiments. The simulation results and the experimental results showed that it could be reduced to the maximum average thrust force when the UVA of LTC vibration is approximately 7 μm . The maximum average thrust force can be reduced by 27% in the case of small UVA, especially in the case of high rotation speed, which is much lower than that of the CD.

Nonetheless, the value of thrust force among all simulation results is almost smaller than the experimental results. The major reason is that the high-frequency vibration of the TDR bit leads to the premature failure of contact elements in the scale-span FE model when the LTC-RUAD process is adopted. In addition, it should be noted that several factors could improve the accuracy of the scale-span FE model, among these are the

use of a more realistic friction model, inclusion of thermal effects, and accounting for TDR wear effects.

4.2 Surface morphology

According to the research by Cheng et al. [32], the microscale damage mechanism of UD-CFRPs is different when different fiber cutting angles are adopted at a microscopic level, which is shown in Fig. 13(b). Yet, in the drilling FE model, it can only show that the stress of the corresponding element is greater in the fiber orientation or elements are deleted because of the limitation of mesh size, which is shown in Figs. 13(c) and 14. Meanwhile, the hole-wall surface also appears to have different damage phenomena because of the different layup angles, such as pits, tears, lateral extrusion, and delamination.

Figure 13 shows the experimental and simulated results of the hole-wall surface morphology using CD and LTC-RUAD. In CD, the lack of the vibration between TDR bit and CFRP workpieces causes the tear, pit, and delamination in the different positions according to the different layups of CFRPs. However, as shown in Fig. 14, due to the effect of repeated vibration ironing using LTC-RUAD, the surface of the drilled hole is smoother than that using CD, and there are only some slight cracks according to

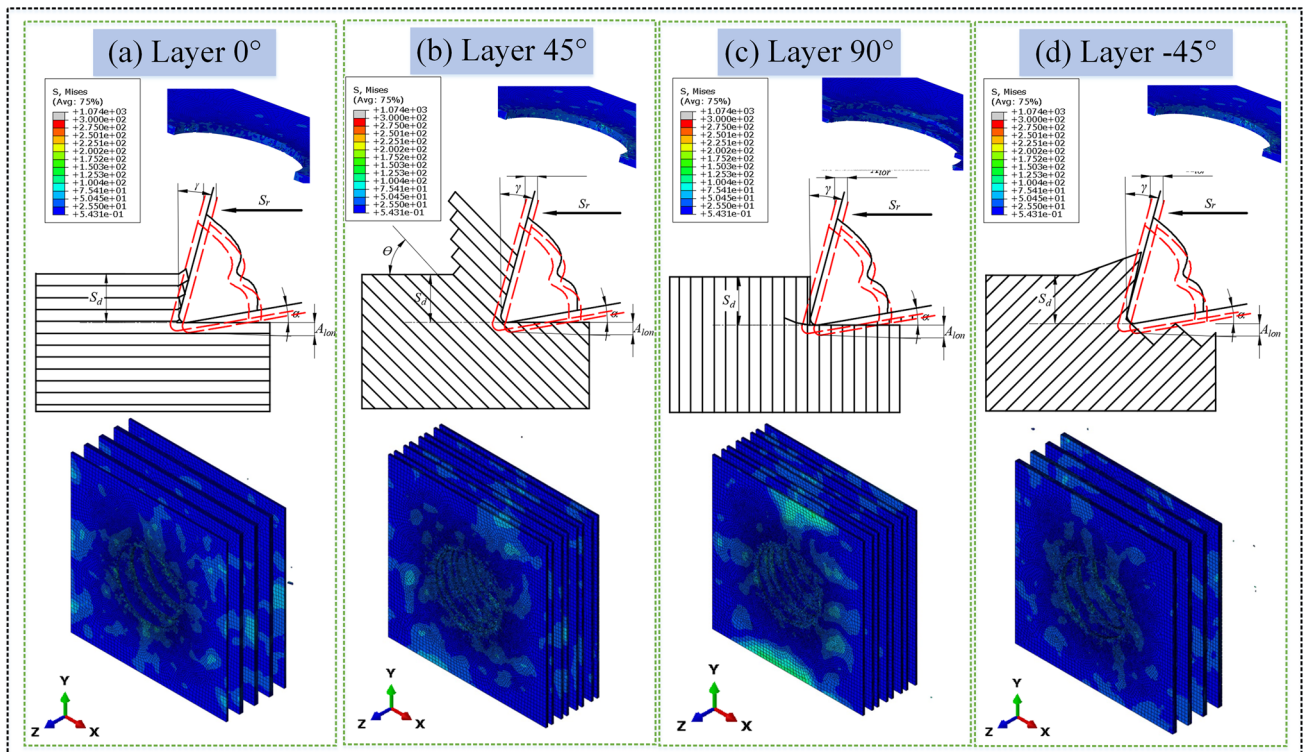


Fig. 14 Damage defects suppression mechanism of CFRPs using LTC-RUAD. (a) Layer 0°. (b) Layer 45°. (c) Layer 90°. (d) Layer -45°

the analysis of the cutting process at the microscale level. Since the damage of the scale-span FE model can only achieve material removal through element deletion or the corresponding stress value become larger, the elements, which are located in the contact areas, can be deleted quickly under the TDR of high-frequency vibration, namely, the fibers can be cut off quickly. Similarly, elements of the scale-span FE model do not reach the maximum damage variable in CD, which promote most of them are retained, whereas the corresponding stress is larger, especially in the bottom layers of CFRPs, which is shown in Fig. 13(c).

In addition, according to the comparative analysis of damage locations of UD-CFRPs with different layups, the damaged positions at which there occurred tear, pits, and delamination of the hole's surface are also consistent with the comparison of the scale-span drilling FE model

and experiments using CD and LTC-RUAD. Therefore, the established scale-span drilling FE model can accurately predict the different kinds of defect state of the CFRP laminate prefabricated hole's surface when the LTC-RUAD process is adopted.

4.3 Entry, exit damage, and delamination

Figure 15 shows the experimental and simulated results of the hole-wall damage morphology at entry and exit using CD and LTC-RUAD. It can be seen that the entrance of the prefabricated hole is relatively flat; only a small amount of tear damage occurred in the experiments. Analogously, the scale-span FE model also shows the similar damage results. However, a large number of burr defect and tear damage appeared in the exit of the hole. Similarly, burr damage phenomena are first simulated in the

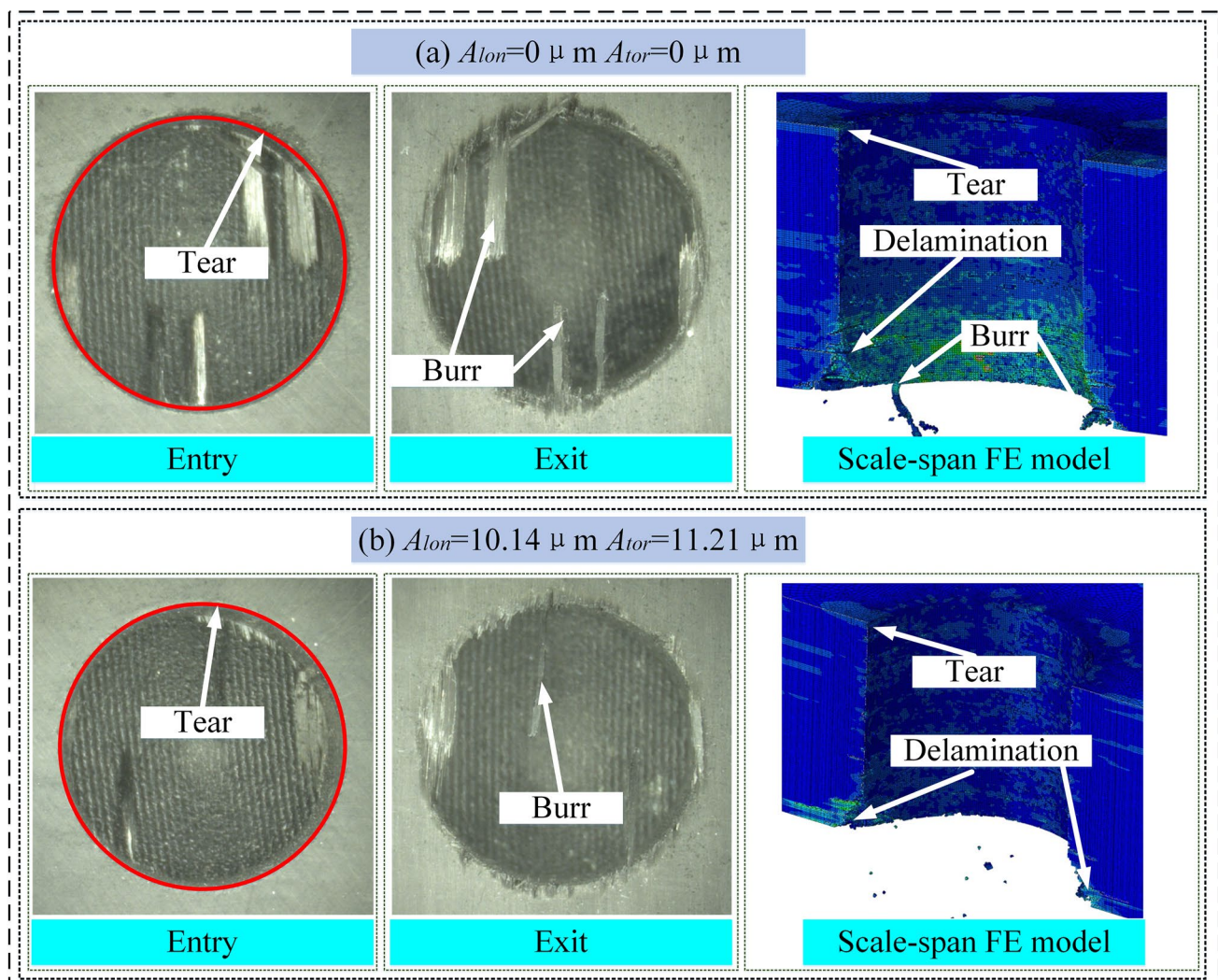


Fig. 15 Comparison of the damage at the entry and exit with CD and LTC-RUAD. (a) $A_{lon}=0 \mu m$, $A_{tor}=0 \mu m$. (b) $A_{lon}=10.14 \mu m$, $A_{tor}=11.21 \mu m$

scale-span FE model, and the damage locations are almost the same, which is shown in Fig. 15(a). Unfortunately, it is difficult to quantify the burr and tear damage owing to the fiber arrangement in species being random, and some initial damage may have existed in the species during preparation, such as microcrack. Meanwhile, in the scale-span FE model that adopts the LTC-RUAD process, the hole-wall precision of the prefabricated hole has been improved obviously, and only minor tearing damage and delamination damage have appeared, which is shown in Fig. 15(b).

Delamination is a serious damage characterized by the separation of UD-CFRP laminate caused by the thrust force. It often initiates at the hole edge and propagates along the fiber direction. The height of the delamination region is higher than the rest of the CFRPs [33]. In order to evaluate the simulation results of scale-span FE model accurately and the delamination damage which can inhibit the delamination using LTC-RUAD, a quantitative analysis of delamination factor at the exit of the hole is adopted in this study. According to Fig. 16(b), the peripheral damage area is assumed as fan-shaped. It is defined as the

ratio of the total peripheral damage area to the nominal hole area.

$$D_d = \left(\frac{A_d}{A_{nom}} - 1 \right) \% \tag{4}$$

where A_d denotes the total area of the delamination zone, and A_{nom} denotes the nominal diameter area.

For the sake of obtaining the value of A_d for the experimental measurement results from all the prefabricated holes, a portion of the uplift height at the exit of the hole is considered delamination area of the specimens, while all the collecting and calculating works were done via SEM, which is shown in Fig. 16(c). For the scale-span FE model, the ratio of the total number of CEs before and after the drilling simulation was calculated using an ABAQUS-Python code script, which is shown in Fig. 17(c). According to the collected average experimental results and the simulation results from different process parameters and UVA, the corresponding delamination factor of drill exit and these absolute percentage deviations [2] are listed in Fig. 18.

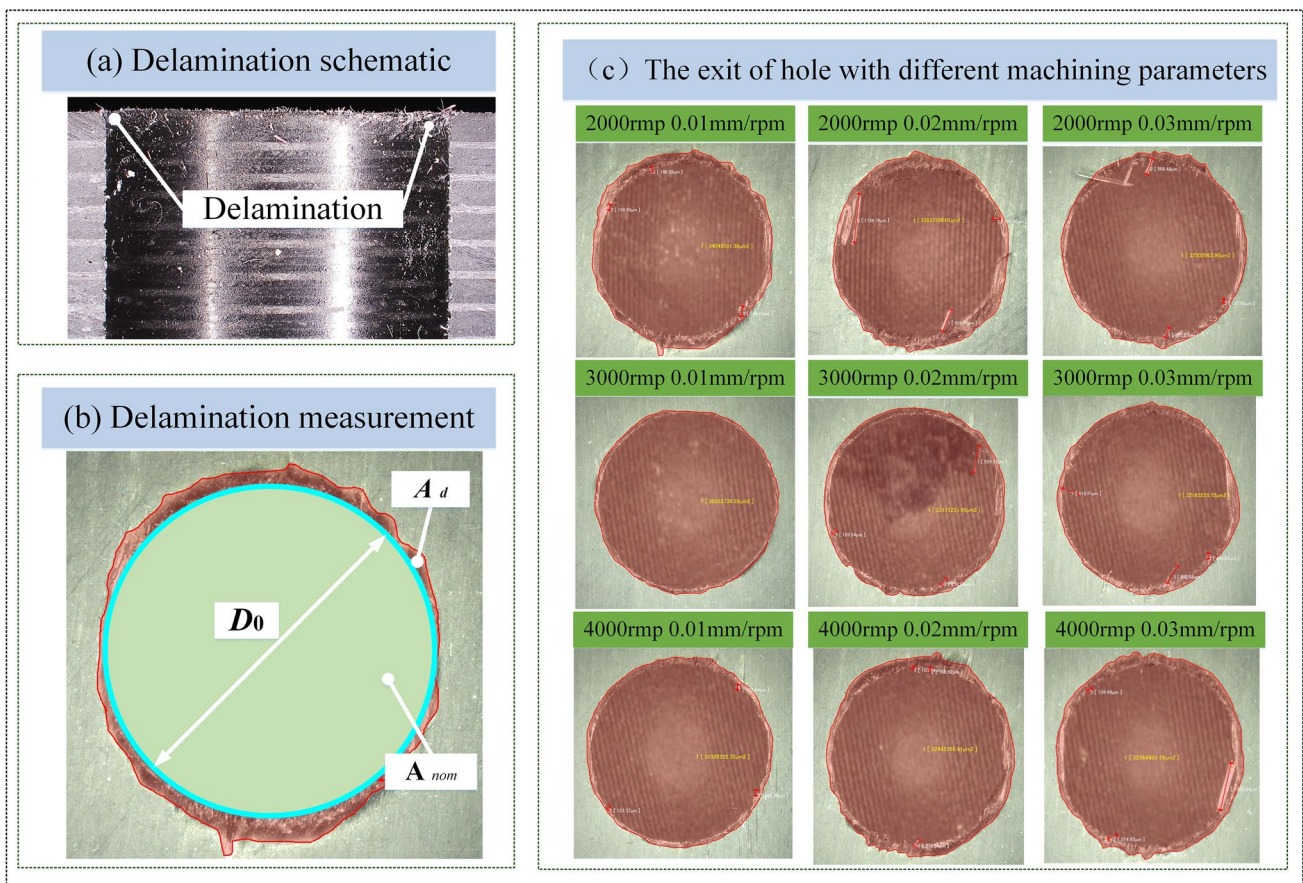


Fig. 16 Measurement of delamination in experiments using LTC-RUAD. (a) Delamination schematic. (b) Delamination measurement. (c) The exit of hole with different machining parameters

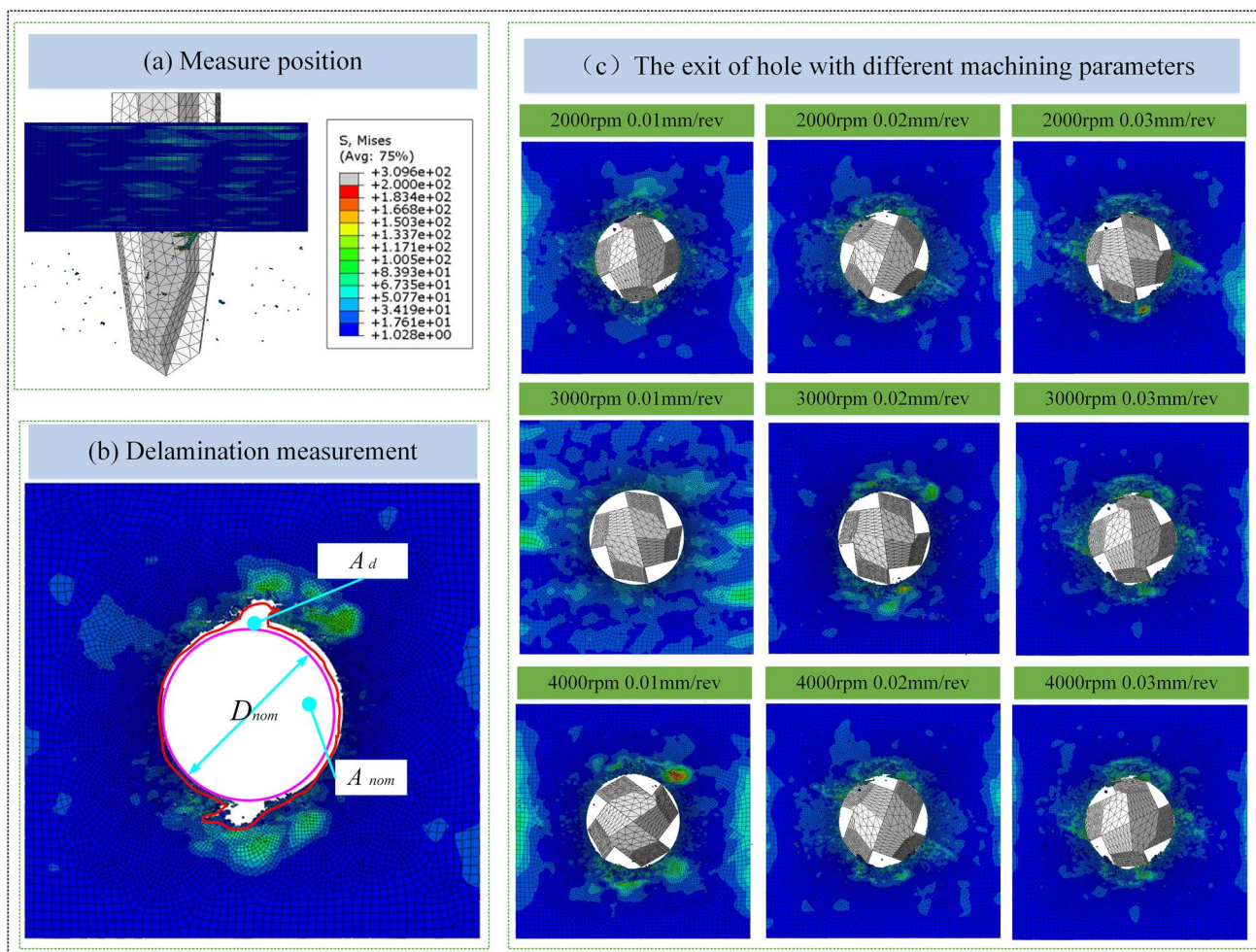


Fig. 17 Measurement of delamination in LTC-RUAD scale-span FE model. (a) Measure position. (b) Delamination measurement. (c) The exit hole with different machining parameters

As can be seen in Fig. 18, the delamination damage behavior at the exit of hole could be realistically predicted via the established scale-span FE model in the drilling of CFRPs using CD and LTC-RUAD. The maximum and

minimum deviation of the delamination factor is approximately 15.69% and 0.37% compared with experiments, respectively. The dominant cause is that there is a material property deviation between the scale-span drilling FE model

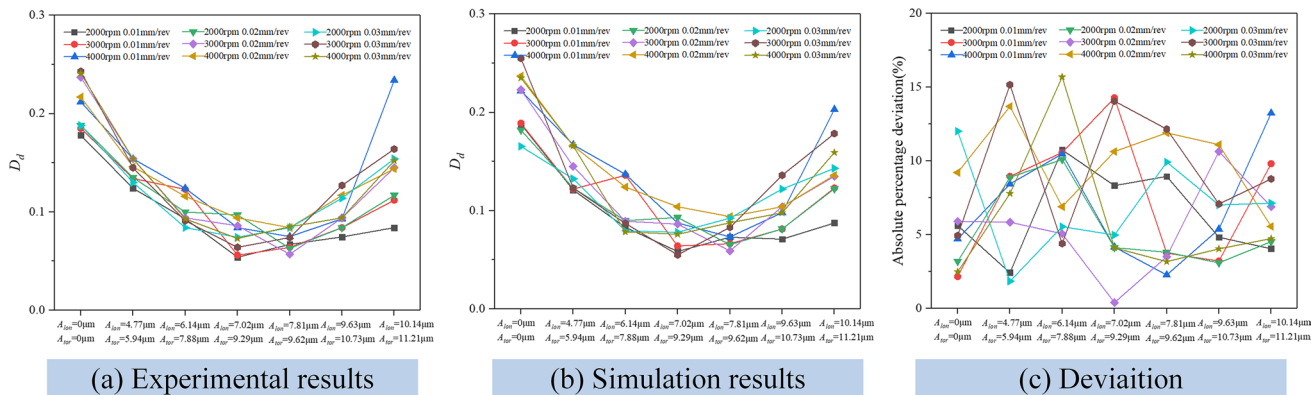


Fig. 18 Comparison of the delamination and deviation (a) Experimental results. (b) Simulation results. (c) Deviation

and experiments under the same machining parameters, followed by the deviation of measurement devices. In addition, the other important reason is that the thermodynamic failure of elements in the drilling process is not taken into account in the established progressive failure theory model.

Although the deviation of obtained simulation results is not regular, the influence of UVA for the suppression of the delamination is almost consistent via the analysis of the simulation results. The delamination factor shows a “concave” trend with the increase of UVA, especially at high rotational speed and low feed rate. The reasons for this case are consistent with the maximum average thrust force; the UVA within the range of 7 μm can cut off the fiber quickly in the case of high frequency owing to its equivalent size to the diameter of fiber. At the same time, it is also verified that the maximum average thrust force is the main factor causing the delamination [33].

Finally, among all experimental and simulation results of scale-span FE model, the quality at the exit of the drilled hole is best when adopting $S_r=2000$ rpm, $S_f=0.01$ mm/rev, $A_{\text{lon}}=7.02$ μm , and $A_{\text{tor}}=9.29$ μm in the LTC-RUAD. The delamination factor is only 0.054, and the damage factors are reduced by 69.67% compared with CD. It is verified that adopting the LTC-RUAD process can greatly restrain the damage of precasted holes in the drilling of CFRPs.

5 Conclusion

In this study, an experiment and scale-span numerical study of drilling in T700S-12 K/YP-H26 CFRPs were presented for both CD and LTC-RUAD process. A drilling experimental platform using the LTC-RUAD was built based on the novel independently designed and manufactured LTC-RUAD vibration actuator, while drilling experiments involving T700S-12 K/YP-H26 CFRP specimens with different process parameters were carried out by modifying the UVA in the longitudinal and torsional directions. Then, a 3D scale-span FE simulation model of CD and LTC-RUAD with different UVAs using TDR bit was developed to find more details about the effects of machining quality on holes. Finally, the defect suppression mechanism of CFRP hole in the LTC-RUAD was revealed via the simulation results from the perspectives of the thrust force and torque, hole-wall surface morphology, and delamination at the hole exit. The main conclusions are obtained as follows:

(1) Predicted thrust force and torque by the scale-span drilling FE model is a reasonable accuracy when compared to experimental results, and the maximum deviations are only 3.43% and 7.69%. The maximum thrust force and torque that adopts LTC-RUAD is greater than that which adopts CD. Nevertheless, the maximum average

thrust force reduction was observed to be as high as 30% under certain drilling conditions.

- (2) Different kinds of damage behavior of holes can be simulated truly in drilling of CFRP laminates using TDR, such as the tear damage at drill entry; pits or lateral extrusion damage at drill surface; and burr, tear, and delamination at drill exit. The maximum thrust force and the delamination factor of drilled hole shows a “concave” trend with the increase of UVA. The corresponding parameters reach the minimum value when the longitudinal UVA is approximately 7–9 μm .
- (3) In LTC-RUAD using the TDR, the quality at the exit of the drilled hole is the best when adopting $S_r=2000$ rpm, $S_f=0.01$ mm/rev, $A_{\text{lon}}=7.02$ μm , and $A_{\text{tor}}=9.29$ μm in the LTC-RUAD. The delamination factor is only 0.054, and the damage factors are reduced by 69.67% compared with CD. In addition, the scale-span FE model was utilized to replicate the drilling process effectively.

Acknowledgements The authors would like to acknowledge the editors and the anonymous referees for their insightful comments.

Author contribution Yong Liu designed the study, performed the research, analyzed the data, and wrote the paper. Zitao Pan and Qiannan Li conducted experiments and data processing. Zhenchao Qi provided experimental condition and directed experiments. Wenliang Chen modified the paper.

Funding Authors declare that we have no financial and personal relationships with other people or organizations that can inappropriately influence our work. The work reported herein is sponsored by the National Natural Science Foundation of China (52105450, 51605221, 51875283), the University Science Research Project of Jiangsu Province (No. 21KJB460016), the Aeronautical Science Foundation of China (2017ZE52052), and the National Commercial Aircraft Manufacturing Engineering Technology Research Center Innovation Foundation (COMAC-SFGS-2019-341).

Availability of data and materials The experimental and simulation data is transparent.

Declarations

Ethics approval This article does not contain any studies with human participants performed by any of the authors.

Consent to participate This work was conducted with no human test subjects.

Consent for publication This work has consent for publication.

Competing interests The authors declare no competing interests.

References

1. Qi Z, Ge E, Yang J, Li F, Jin S (2021) Influence mechanism of multi-factor on the diameter of the stepped hole in the drilling of CFRP/Ti stacks. *Int J Adv Manuf Technol* 113:923–933

2. Liu Y, Qi Z, Chen W, Wang X (2019) An approach to design high-performance unidirectional CFRPs based on a new sensitivity analysis model *Compos Struct* 224:111078.
3. Abhishek K, Datta S, Mahapatra SS (2014) Optimization of thrust, torque, entry, and exist delamination factor during drilling of CFRP composites. *Int J Adv Manuf Technol* 76(1–4):401–416
4. Geng D, Liu Y, Shao Z, Lu Z, Cai J, Li X, Jiang X, Zhang D (2019) Delamination formation, evaluation and suppression during drilling of composite laminates: a review. *Compos Struct* 216:168–186
5. Geng D, Teng Y, Liu Y, Shao Z, Jiang X, Zhang D (2019) Experimental study on drilling load and hole quality during rotary ultrasonic helical machining of small-diameter CFRP holes. *J Mater Process Technol* 270:195–205
6. Chen Y, Su H, Qian N, He J, Ding K (2021) Ultrasonic vibration-assisted grinding of silicon carbide ceramics based on actual amplitude measurement: grinding force and surface quality. *Ceram Int* 47:15433–15441
7. Zhang D, Wang H, Burks AR, Cong W (2020) Delamination in rotary ultrasonic machining of CFRP composites: finite element analysis and experimental implementation. *Int J Adv Manuf Technol* 107(1):1–12
8. Liu Y, Li Q, Qi Z, Chen W (2021a) Defect suppression mechanism and experimental study on longitudinal torsional coupled rotary ultrasonic assisted drilling of CFRPs. *J Manuf Process* 70:177–192. <https://doi.org/10.1016/j.jmapro.2021.08.042>
9. Wang J, Zhang J, Feng P, Ping Q (2018) Feasibility study of longitudinal torsional coupled rotary ultrasonic machining of brittle material. *J. Eng. Ind.* 140(5): 051008.
10. Wang J, Feng P, Zhang J, Guo P (2018) Reducing cutting force in rotary ultrasonic drilling of ceramic matrix composites with longitudinal-torsional coupled vibration. *Manuf. Lett.* 18:1–5
11. Sadek A, Attia MH, Meshreki M, Shi B (2013) Characterization and optimization of vibration-assisted drilling of fibre reinforced epoxy laminates. *CIRP Ann Manuf Technol* 62(1):91–94
12. Cong WL, Pei ZJ, Sun X, Zhang C (2014) Rotary ultrasonic machining of CFRP: a mechanistic predictive model for cutting force. *Ultrasonics* 54(2):663–675
13. Wang H, Ning F, Li Y, Hu Y, Cong W (2019) Scratching-induced surface characteristics and material removal mechanisms in rotary ultrasonic surface machining of CFRP. *Ultrasonics* 97:19–28
14. Wang H, Hu Y, Cong W, Burks A (2019) Rotary ultrasonic machining of carbon fiber-reinforced plastic composites: effects of ultrasonic frequency. *Int J Adv Manuf Technol* 104(3):3759–3772
15. Thomas PNH, Babitsky VI (2017) Experiments and simulations on ultrasonically assisted drilling. *J Sound Vib* 308(3–5):815–830
16. Makhdam F, Phadnis VA, Roy A, Silberschmidt V (2014) Effect of ultrasonically-assisted drilling on carbon-fibre-reinforced plastics. *J Sound Vib* 333(23):5939–5952
17. Asami T, Miura H (2015) Study of ultrasonic machining using longitudinal and torsional vibration, 2015 IEEE International Ultrasonics Symposium (IUS). IEEE.
18. Lotfi M, Amini S (2016) Effect of ultrasonic vibration on frictional behavior of tool–chip interface: finite element analysis and experimental study. *Proc. Inst. Mech. Eng., Part B* 7:1212–1220
19. Phadnis VA, Makhdam F, Roy A, Silberschmidt V (2012) Experimental and numerical investigations in conventional and ultrasonically assisted drilling of CFRP laminate. *Procedia Cirp* 1(7):455–459
20. Phadnis VA, Roy A, Silberschmidt VV (2013) A finite element model of ultrasonically assisted drilling in carbon/epoxy composites. *Procedia CIRP* 8(1):141–146
21. Gomes GF, Diniz CA, Da Cunha SS, Anceletti AC (2017) Design optimization of composite prosthetic tubes using GA-ANN algorithm considering Tsai-Wu failure criteria. *J Fail Anal Prev* 17:740–749
22. Hashin Z, Rotem A (1973) A fatigue failure criterion for fiber reinforced materials. *J Compos Mater* 7(4):448–464
23. Hashin Z (1981) Fatigue failure criteria for unidirectional fiber composites. *J Appl Mech* 48(4):846
24. Puck AH (2002) Schürmann. Failure analysis of FRP laminates by means of physically based phenomenological models. *Compos Sci Technol* 62:1633–1662
25. Chang FK, Chang KY (1987) A progressive damage model for laminated composites containing stress concentrations. *J Compos Mater* 21(9):834–855
26. Ma X, Li Y, Gu Y, Li M, Zhang Z (2014) Numerical simulation of prepreg resin impregnation effect in vacuum-assisted resin infusion/prepreg co-curing process. *J Reinf Plast Compos* 33:2265–2273
27. Tsao CC, Hocheng H (2008) Evaluation of thrust force and surface roughness in drilling composite material using Taguchi analysis and neural network. *J Mater Process Technol* 203(1–3):342–348
28. Wang F, Qian B, Jia Z, Cheng D, Fu R (2018) Effects of cooling position on tool wear reduction of secondary cutting edge corner of one-shot drill bit in drilling CFRP. *Int J Adv Manuf Technol* 94:4277–4287
29. Liu Y, Li Q, Qi Z, Chen W (2021b) Scale-span modelling of dynamic progressive failure in drilling CFRPs using a tapered drill-reamer. *Compos Struct* 278:114710. <https://doi.org/10.1016/j.compstruct.2021.114710>
30. Qi Z, Liu Y, Chen W (2019) An approach to predict the mechanical properties of CFRP based on cross-scale simulation. *Compos Struct* 210:339–347
31. Ducobu F, Rivière-Lorphèvre E, Filippi E (2015) On the introduction of adaptive mass scaling in a finite element model of Ti6Al4V orthogonal cutting. *Simul Model Pract Theory* 53:1–14
32. Chen L, Zhang K, Hui C, Qi Z, Meng Q (2017) A cutting force predicting model in orthogonal machining of unidirectional CFRP for entire range of fiber orientation. *Int J Adv Manuf Technol* 89(1–4):1–14
33. Faraz A, Biermann D, Weinert K (2009) Cutting edge rounding: an innovative tool wear criterion in drilling CFRP composite laminates. *Int J Mach Tools Manuf* 49(15):1185–1196

Publisher's Note Springer Nature remains neutral with regard to jurisdictional claims in published maps and institutional affiliations.